COMMUNICATIONS IN COMPUTATIONAL PHYSICS
Vol. **2**, No. 1, pp. 54-72

Commun. Comput. Phys.
February 2007

An Efficient Spectral Method for Acoustic Scattering from Rough Surfaces

Dongbin Xiu* and Jie Shen

Department of Mathematics, Purdue University, West Lafayette, IN 47907, USA.

Received 3 February 2006; Accepted (in revised version) 9 May 2006

Available online 30 August 2006

Abstract. An efficient and accurate spectral method is presented for scattering problems with rough surfaces. A probabilistic framework is adopted by modeling the surface roughness as random process. An improved boundary perturbation technique is employed to transform the original Helmholtz equation in a random domain into a stochastic Helmholtz equation in a fixed domain. The generalized polynomial chaos (gPC) is then used to discretize the random space; and a Fourier-Legendre method to discretize the physical space. These result in a highly efficient and accurate spectral algorithm for acoustic scattering from rough surfaces. Numerical examples are presented to illustrate the accuracy and efficiency of the present algorithm.

AMS subject classfications: 65C20, 65C30, 78A45, 35J05

Key words: Acoustic scattering; spectral methods, stochastic inputs, differential equations, uncertainty quantification.

1 Introduction

Wave scattering from (random) rough surfaces is a very common physical phenomenon and is at the core of a variety of technologies ranging from SAR imaging and remote sensing to underwater acoustics, optical lithography, and meteorology. The design of numerical methods to faithfully simulate such scattering processes presents significant challenges, largely due to the need to resolve wave oscillations and interactions, and in many cases, high accuracy requirements.

A wide variety of techniques have been proposed for wave scattering from irregular obstacles, e.g., small-slope approximation, Kirchhoff approximation, momentum transfer expansion, etc. (see the survey paper [25] and the references therein). Among the most compelling of these are those based on boundary perturbations which can be traced

*Corresponding author. *Email addresses:* dxiu@math.purdue.edu (D. Xiu), shen@math.purdue.edu (J. Shen)

to the work of Rayleigh [16] and Rice [17]. These methods are fast, straightforward to implement, and quite accurate within their domain of applicability. It has been shown rigorously that the scattered fields are analytical functions of the grating height (slope) parameter ([2, 8]), and this provides justifications for boundary perturbations. However, the traditional approaches of [16, 17] become *ill-conditioned* at high orders because they rely on significant cancellations for convergence ([12, 13]). Subsequently, an improved boundary perturbation algorithm was proposed in [13] to overcome the issue of poor conditioning. This method, termed "Transformed Field Expansions" (TFE), employs a change of variables which "flattens" the shape of the scatter to a flat configuration and is shown to be accurate and robust at high orders. In [14], the TFE technique is combined with a highly efficient spectral Galerkin method in polar coordinates and applied to bounded obstacles. Extensive numerical experiments were conducted to demonstrate the efficiency and accuracy of the method.

Due to the lack of knowledge and/or measurement of realistic rough surfaces, it is natural to adopt a probabilistic framework, where rough surfaces are modeled as random processes which are typically characterized by surface height probability distributions and their cross correlations. Most of the existing numerical approaches adopt one of the afore-mentioned methods for a single deterministic irregular surface. Statistical averaging is then applied over an ensemble of such deterministic simulations to generate probabilistic information of the scattered fields, e.g., mean, standard deviation, etc. This is the classical Monte Carlo type procedure and can be computationally intensive as the convergence rate of the statistics is relatively slow, e.g., the mean field usually converges as $1/\sqrt{K}$ where K is the number of realizations. A large solution ensemble involving many realizations of deterministic simulations are required to obtain sufficiently accurate solution statistics. Recently, a high-order non-sampling method based on Generalized Polynomial Chaos (gPC) was developed for differential equations with random inputs [29]. It is a generalization of the Wiener-Hermite expansion [26] and is essentially a spectral approximation of functionals in random space. The basis functions include global orthogonal polynomials [4, 5, 29], piecewise polynomials [1], and wavelets [6]. Along with Galerkin projection, the resulting stochastic Galerkin (SG) algorithm can be highly efficient in many applications with random initial/boundary conditions, uncertain parameters, etc. See, for example, [28, 30] for numerical examples, [1] for analysis on elliptic equations and [3] on Burgers' equation.

Stochastic modeling in (random) rough domains, despite its practical and theoretical importance, is relatively underdeveloped. Efficient numerical algorithms using gPC expansions were developed in [31] and [24], where a robust numerical mapping and an analytical mapping, respectively, were employed to transform the problems into fixed domains. In this paper, we extend the TFE boundary perturbation method to scattering of *random rough surfaces*. The surfaces are to be modeled as random processes and the resulting governing equations, Helmholtz equation for acoustic scattering, become stochastic partial differential equations. The gPC expansion is employed as a spectral method in random space, and a Galerkin method is used to obtain the governing equations for the

gPC expansion coefficients. A high-order stochastic collocation method ([27]) is also employed to facilitate the Galerkin projection of the right-hand-side, which takes a complicated form in this case, of the governing stochastic Helmholtz equations. The resulting equations are *deterministic* and standard numerical techniques can be applied. We will focus, in this paper, acoustic scattering of two-dimensional bounded obstacles. A highly efficient spectral-Galerkin method will be used as spatial discretization in physical space. Such a method was developed for elliptic equations in bounded domains in [19–21] and was recently extended to the Helmholtz equation in exterior domains through the Dirichlet-to-Neumann operator [14]. The overall algorithm is a unified spectral method for scattering problems over random rough surfaces. It yields spectral accuracy in both physical space and random space.

In the next section we will present the mathematical formulations in stochastic framework. Details of numerical procedures will be presented in Section 3. Several numerical examples are given in Section 4 to illustrate convergence and efficiency of the new algorithm. we summarize the paper in Section 5.

2 Mathematical formulations

In this study we will focus on the problem of solving electromagnetic and acoustic plane-wave scattering from bounded obstacles with rough boundaries. For simplicity we restrict our attention to the scalar case in two dimensions, and leave the more general three dimensional setting for future work.

2.1 Deterministic governing equations

Let us assume that

$$D=\{(r,\theta):r\leq a+\widetilde{g}(\theta),0\leq\theta<2\pi\} \tag{2.1}$$

is a bounded domain in $\mathbb{R}^2$ representing an impenetrable body with boundary $\partial D=\{(r,\theta):r=a+\widetilde{g}(\theta),0\leq\theta\leq 2\pi\}$. For an incident time-harmonic (plane) wave v^{inc} illuminating the scatterer in an isotropic medium, the diffracted field v satisfies the following exterior boundary value problem:

$$\Delta v+k^2v=0, \qquad r<a+\widetilde{g}(\theta), \tag{2.2a}$$

$$v=\xi \text{ or } \partial_n v=\xi, \qquad r=a+\widetilde{g}(\theta), \tag{2.2b}$$

$$\lim_{r\to\infty} r^{1/2}(\partial_r v-ikv)=0, \qquad r\to\infty, \tag{2.2c}$$

where k is the wavenumber and n is the unit outward normal. The boundary condition depends on the physical problem — it is Dirichlet for sound-soft problems and Neumann for sound-hard problems. Finally, the Sommerfeld radiation condition is imposed at infinity. For notational convenience, we will restrict our discussions to the Dirichlet case in the following.

An equivalent statement which poses the problem on a *bounded* domain can be made in terms of the Dirichlet–Neumann operator (DNO), also called the Dirichlet–to–Neumann (DtN) map. Let $b>a+|\widetilde{g}|_{L^\infty}$, then, using a classical argument of separation of variables, the general solution of (2.2a)–(2.2c) for $r\geq b$ can be expressed as

$$v(r,\theta)=\sum_{p=-\infty}^{\infty}a_pH_p^{(1)}(kr)e^{ip\theta},$$

where $H_p^{(1)}$ is the p-th degree Hankel function of the first kind. Therefore, if $v(b,\theta)$ is given, we can write

$$v(b,\theta)=\psi(\theta)=\sum_{p=-\infty}^{\infty}\hat{\psi}_pe^{ip\theta}.$$

Hence, the coefficients $\{a_p\}$ can be uniquely determined, namely, we have

$$v(r,\theta)=\sum_{p=-\infty}^{\infty}\hat{\psi}_p\frac{H_p^{(1)}(kr)}{H_p^{(1)}(kb)}e^{ip\theta}.$$

We now define the Dirichlet–to–Neumann operator T by

$$T\psi\equiv\partial_rv(b,\theta)=\sum_{p=-\infty}^{\infty}k\frac{d_zH_p^{(1)}(kb)}{H_p^{(1)}(kb)}\hat{\psi}_pe^{ip\theta},\tag{2.3}$$

where

$$d_zH_p^{(1)}(kb)=\left.\frac{dH_p^{(1)}(z)}{dz}\right|_{z=kb},$$

which maps the Dirichlet data ψ to the Neumann data $\partial_rv|_{r=b}$. Thus, (2.2) can be equivalently restated as

$$\Delta v+k^2v=0,\qquad (r,\theta)\in D_{a+\widetilde{g},b},\tag{2.4a}$$
$$v(a+\widetilde{g}(\theta),\theta)=\xi(\theta),\tag{2.4b}$$
$$\partial_rv(b,\theta)-Tv(b,\theta)=0.\tag{2.4c}$$

where

$$D_{a+\widetilde{g},b}=\{(r,\theta):a+\widetilde{g}(\theta)<r<b,0\leq\theta<2\pi\}.$$

2.2 Probabilistic modeling of rough surfaces

To incorporate the ubiquitous uncertainty and geometrical "imperfection" in realistic scatter surfaces, we adopt a probabilistic setting and model the surfaces as random processes. Let $(\Omega,\mathcal{A},\mathcal{P})$ be a properly defined complete probability space, where Ω is the

event space, $\mathcal{A}$ its σ-algebra, and $\mathcal{P}$ a probability measure. We consider, for $\mathcal{P}$-a.e. $\omega\in\Omega$, the following random domain

$$D(\omega)=\{(r,\theta,\omega):r\leq a+\widetilde{g}(\theta,\omega),0\leq\theta<2\pi\}, \tag{2.5}$$

where $\widetilde{g}(\theta,\omega)$ is a random process characterizing the geometrical uncertainty of the scatter boundary. For any fixed ω, $\widetilde{g}(\theta,\cdot)$ is a deterministic function representing a *realization* of the surface geometry; and at a given location with fixed θ, $\widetilde{g}(\cdot,\omega)$ is a *random variable* representing the uncertain height of the surface at this location.

For numerical simulations, continuous random processes such as $\widetilde{g}(\theta,\omega)$ need to be discretized. This is accomplished by representing/approximating $\widetilde{g}(\cdot,\omega)$ by a function with only *finite number of random variables*, i.e.,

$$\widetilde{g}(\theta,\omega)\approx g(\theta,Y^1(\omega),\ldots,Y^N(\omega)), \tag{2.6}$$

where $\{Y^n(\omega)\}_{n=1}^N$ is a set of *mutually independent* random variables. The requirement of independence is essential for numerical simulations, because most, if not all, random number generators nowadays generate *independent* series of random numbers.

Gaussian processes can be completely specified by their first two moments (mean and covariance functions), and their finite-term approximation procedure (2.6) is relatively straightforward. The most widely used methods are spectral expansion [22] and Karhunen-Loève (KL) expansion [7]. In spectral methods a Gaussian process is expressed as a finite-term Fourier series with uncorrelated Gaussian random frequency whose amplitudes are determined by matching the power spectra of the process, while in KL expansion a Gaussian process is approximated by a finite-term summation of the eigenfunctions of its covariance function with uncorrelated Gaussian random coefficients. (Note that for Gaussian distribution, independence is equivalent to uncorrelation.)

Although both the spectral method and the KL expansion work well for Gaussian processes where the dominating approximation errors stem from the finite-term truncations, it is much more challenging to simulate non-Gaussian processes, whose complete specifications involve all joint probability distributions at all locations in physical space. The task is often reduced to matching only the pointwise marginal distributions at given locations in physical space and their cross-correlations. Typical methods are often based on iterative corrections to spectral expansion (e.g., [32]) or KL expansion (e.g. [18]). Many issues are still under investigation and belong to the topic of "digital generations of non-Gaussian random fields", which remains an active research field.

In this paper we will assume that a satisfactory representation/approximation of a given random surface in the form of (2.6) has been established, and the errors associated with the model been quantified. The actual procedure to obtain (2.6) is beyond the scope of this paper and the readers are referred to [18, 32], and the references therein, for more details.

Let $\rho_i:\Gamma^i\to\mathbb{R}^+$ be the probability density functions of the random variable $Y^i(\omega)$, and

its image $\Gamma^i \equiv Y^i(\Omega) \in \mathbb{R}$ be intervals in $\mathbb{R}$ for $i=1,\ldots,N$. Then

$$\rho(y) = \prod_{i=1}^{N} \rho_i(Y^i), \qquad \forall y \in \Gamma \tag{2.7}$$

is the joint probability density of the random vector $y=(Y^1,\cdots,Y^N)$ with the support

$$\Gamma \equiv \prod_{i=1}^{N} \Gamma^i \subset \mathbb{R}^N. \tag{2.8}$$

This allows us to conduct numerical formulations in a finite dimensional (N-dimensional) random space Γ, in replacement of the infinite dimensional space Ω.

2.3 Stochastic governing equations

The computational domain of interest now becomes

$$D(\omega) = \{(r,\theta,y(\omega)) : r \le a+g(\theta,y(\omega)), 0 \le \theta < 2\pi\}, \tag{2.9}$$

where

$$y(\omega) = (Y^1(\omega,\ldots,Y^N(\omega))$$

is the finite-variate random vector in (2.6) whose components are mutually independent. According to Doob-Dynkin lemma [15], the scattered field is also a function of this finite-variate random vector. The stochastic version of the governing equations are, for all $y(\omega) \in \Gamma$,

$$\Delta v(r,\theta,y) + k^2 v(r,\theta,y) = 0, \qquad (r,\theta) \in D_{a+g,b}(\omega), \tag{2.10a}$$

$$v(a+g(\theta,y),\theta) = \xi(\theta), \tag{2.10b}$$

$$\partial_r v(b,\theta,y) - Tv(b,\theta,y) = 0. \tag{2.10c}$$

where

$$D_{a+g,b}(\omega) = \{(r,\theta,y(\omega)) : a+g(\theta,y(\omega)) < r < b, 0 \le \theta < 2\pi\}.$$

Note that the only randomness is from the uncertain geometry of the domain $D(\omega)$.

3 Numerical methods

In what follows, we consider sufficiently smooth (random) boundary deformations of the form $g(\theta,y(\omega)) = \varepsilon f(\theta,y(\omega))$, where $|f|_{L^\infty} \sim \mathcal{O}(1)$ for all $y(\omega)$ and $0<\varepsilon<1$ controls the amplitude of boundary perturbation. Following [2, 8, 12, 13], the scattered field v depends analytically on the parameter ε, and we have a strongly convergent expansion, for all $y \in \Gamma$,

$$v(r,\theta,y(\omega);\varepsilon) = \sum_{n=0}^{\infty} v_n(r,\theta,y) \cdot \varepsilon^n. \tag{3.1}$$

Our numerical procedure for system (2.10) consists of three essential steps: (i) using the Transformed Field Expansion (TFE) to derive the (stochastic) governing equations for $\{v_n\}$; (ii) using the generalized Polynomial Chaos (gPC) expansion along with stochastic Galerkin (SG) and stochastic collocation (SC) methods to convert the stochastic equations for $\{v_n\}$ to a set of deterministic governing equations; and (iii) solving these deterministic equations by an efficient spectral method in physical space.

3.1 Transformed field expansion

The idea behind the traditional "field expansion" (FE) method is to solve $\{v_n\}$ in (3.1) recursively as solutions of a sequence of Helmholtz problems in the unperturbed domain

$$D_{a,b}=\{(r,\theta):a<r<b,0\leq\theta<2\pi\}.$$

As shown in [12,13], such an approach suffers from severe ill-conditioning at high orders due to significant cancellations in the recursion. As a remedy, the "transformed field expansion" (TFE) was developed in [8–13], where a change of variables coupled to the FE design leads to a stable and robust high-order boundary perturbation scheme. The change of variables takes the following form, for all $y\in\Gamma$,

$$r'=\frac{(b-a)r-bg(\theta)}{(b-a)-g(\theta)}=\frac{dr-bg}{d-g},\qquad \theta'=\theta,$$

where $d=(b-a)$, maps the perturbed geometry $D_{a+g,b}$ to the annulus $D_{a,b}$. The governing equation (2.10) in these transformed coordinates becomes, upon dropping the primes in (r',θ'),

$$D_r^2u+\partial_\theta^2u+r^2k^2u=F(r,\theta,y;u),\qquad (r,\theta)\in D_{a,b}, \tag{3.2a}$$
$$u(a,\theta,y)=\xi(\theta), \tag{3.2b}$$
$$\partial_r u(b,\theta,y)-Tu(b,\theta,y)=J(\theta,y), \tag{3.2c}$$

where $D_r=r\partial_r$,

$$\begin{aligned}
&u(r,\theta,y)=v(r+A/d,\theta,y),\qquad dJ(\theta,y)=-g(\theta,y)Tu(b,\theta,y).\\
&-d^2F=dA\partial_rD_ru+dD_r[A\partial_ru]+A\partial_r[A\partial_ru]\\
&\qquad -dg\partial_\theta^2u-d\partial_\theta[g\partial_\theta u]+g\partial_\theta[g\partial_\theta u]-dB\partial_r\partial_\theta u+B\partial_r[g\partial_\theta u]\\
&\qquad -d\partial_\theta[B\partial_ru]+g\partial_\theta[B\partial_ru]+B\partial_r[B\partial_ru]\\
&\qquad +d(\partial_\theta g)\partial_\theta u-g(\partial_\theta g)\partial_\theta u-(\partial_\theta g)B\partial_ru+\sum_{j=1}^{4}C_j(g)k^2u,\\
&A(r,\theta,y)=g(\theta,y)(b-r),\qquad B(r,\theta,y)=\partial_\theta A=(\partial_\theta g(\theta,y))(b-r),
\end{aligned}$$

and

$$\begin{aligned}
C_1(g) &= -2d\ g(r)^2 + 2d\ Ar,\\
C_2(g) &= g^2(r)^2 - 4gAr + A^2,\\
C_3(g) &= (2/d)Ag^2r - (2/d)gA^2,\\
C_4(g) &= (1/d^2)g^2A^2.
\end{aligned}$$

Note that the transformation converts (2.10), a deterministic problem in a random domain, to (3.2), a stochastic problem in a fixed domain. More details on the transformation can be found in [14].

Again, letting $g=\varepsilon f$, for f sufficiently smooth, the analyticity of the *transformed* field u (see [8]) implies that

$$u(r,\theta,y;\varepsilon) = \sum_{n=0}^{n_{\max}} u_n(r,\theta,y)\ \varepsilon^n, \qquad n_{\max}\to\infty. \tag{3.3}$$

Inserting the above in (3.2), it is straightforward, albeit tedious, to derive the following recursions, for $\{u_n\}$: for all $y\in\Gamma$,

$$D_r^2 u_n + \partial_\theta^2 u_n + r^2k^2u_n = F_n(r,\theta,y), \qquad (r,\theta)\in D_{a,b}, \tag{3.4a}$$

$$u_n(a,\theta,y) = \delta_{n,0}\ \xi(\theta), \tag{3.4b}$$

$$\partial_r u_n(b,\theta,y) - Tu_n(b,\theta,y) = J_n(\theta,y), \tag{3.4c}$$

where

$$\begin{aligned}
-d^2F_n =& dA\partial_r D_r u_{n-1} + dDr[A\partial_r u_{n-1}] + A\partial_r[A\partial_r u_{n-2}] - df\partial_\theta^2 u_{n-1}\\
&- d\partial_\theta[f\partial_\theta u_{n-1}] + f\partial_\theta[f\partial_\theta u_{n-2}] - dB\partial_r\partial_\theta u_{n-1} + B\partial_r[f\partial_\theta u_{n-2}]\\
&- d\partial_\theta[B\partial_r u_{n-1}] + f\partial_\theta[B\partial_r u_{n-2}] + B\partial_r[B\partial_r u_{n-2}]\\
&+ d(\partial_\theta f)\partial_\theta u_{n-1} - f(\partial_\theta f)\partial_\theta u_{n-2} - (\partial_\theta f)B\partial_r u_{n-2} + \sum_{j=1}^{4} C_j(f)k^2 u_{n-j},
\end{aligned} \tag{3.4d}$$

$$dJ_n = -fTu_{n-1}(b,\theta,y). \tag{3.4e}$$

For details of the derivation, see [14].

3.2 Spectral discretizations in random space: gPC

In the finite dimensional random space Γ defined in (2.8), the gPC expansion seeks to approximate a random function via orthogonal polynomials of random variables. Let us define one-dimensional orthogonal polynomial spaces with respect to the measure $\rho_i(Y^i)dy$ in $\Gamma^i, i=1,\ldots,N$,

$$W^{i,p_i} \equiv \left\{ v:\Gamma^i\to\mathbb{R} : v\in \operatorname{span}\left\{\phi_m(Y^i)\right\}_{m=0}^{p_i} \right\}, \qquad i=1,\cdots,N, \tag{3.5}$$

where $\{\phi_m(Y^i)\}$ are a set of orthogonal polynomials satisfying the orthogonality conditions

$$\int_{\Gamma_i} \rho_i(Y^i)\phi_m(Y^i)\phi_n(Y^i)dY^i = h_m^2\delta_{mn}, \tag{3.6}$$

with normalization factors $h_m^2 = \int_{\Gamma_i}\rho_i\phi_m^2 dY^i$. The type of the orthogonal polynomials $\{\phi_m(Y^i)\}$ in (3.6) is determined by $\rho_i(Y^i)$, the probability density function of $Y^i(\omega)$, for $i=1,\cdots,N$. For example, uniform distributions are associated with Legendre polynomials, and Gaussian distributions are associated with Hermite polynomials. (See [28,29] for a detailed list of correspondences.)

The corresponding N-variate orthogonal polynomial space in Γ is defined as

$$W_N^P \equiv \bigotimes_{|\mathbf{p}|\le P} W^{i,p_i}, \tag{3.7}$$

where the tensor product is over all possible combinations of the multi-index $\mathbf{p}=(p_1,\cdots,p_N)\in\mathbb{N}_0^N$ satisfying $|\mathbf{p}| = \sum_{i=1}^N p_i \le P$. Thus, W_N^P is the space of N-variate orthogonal polynomials of total degree at most P, and the number of basis functions in (3.7) is $\dim(W_N^P)=\binom{N+P}{N}$. Such spaces are often employed in the (generalized) polynomial chaos expansions [5,28,30].

The finite order, P^{th}-order, gPC approximation of a given function in $v(y)$ in the space Γ is

$$v_N^P(y) = \sum_{m=1}^M \hat{v}_m\Phi_m(y), \qquad M=\binom{N+P}{N}, \tag{3.8}$$

where

$$\hat{v}_m = \frac{1}{h_m^2}\int_\Gamma v(y)\Phi_m(y)\rho(y)dy, \qquad m=1,\ldots,M.$$

The convergence of $\|v-v_N^P\|_{L^2_\rho(\Gamma)}$ depends on the regularity of $v(y)$, and can be very fast when $v(y)$ is sufficiently smooth. For low to moderate value of N, stochastic Galerkin methods are preferred because their high accuracy and fast convergence; and for large value of $N\gg 1$, the rapidly growing number of basis functions effectively reduces its efficiency. In this case, the Monte Carlo method should be considered. However, if a highly accurate stochastic solution is desired, then stochastic Galerkin methods can be more efficient even for relatively large values of N. (This was shown rigorously in [1], and demonstrated numerically for $N>20$ in [27,31]).

3.2.1 gPC Galerkin approach for governing equations

The stochastic Galerkin method for a stochastic differential equation like (3.4) is better illustrated in the following general form. For a given stochastic boundary value problem,

$$\mathcal{L}(y,x;u) = s(y,x), \qquad (y,x)\in\Gamma\times D, \tag{3.9}$$

subject to the boundary condition

$$\mathcal{B}(y,x;u)=r(y,x), \qquad (y,x)\in\Gamma\times\partial D, \tag{3.10}$$

where $\mathcal{B}$ is the boundary condition operator. We seek $u_N^P(y,x)\in W_N^P(y)$ such that

$$\int_\Gamma \rho(y)\mathcal{L}\left(y,x;u_N^P\right)v(y)dy=\int_\Gamma \rho(y)s(y,x)v(y)dy, \forall v(y)\in W_N^P, x\in D, \tag{3.11}$$

$$\int_\Gamma \rho(y)\mathcal{B}(y,x,u_N^P)v(y)dy=\int_\Gamma \rho(y)r(y,x)v(y)dy, \forall v(y)\in W_N^P, x\in\partial D \tag{3.12}$$

The resulting problem (3.11)–(3.12) thus becomes a deterministic problem in the physical domain D, and can be solved by a standard discretization technique, e.g., finite elements, finite volume, etc.

In the TFE approach (3.3)–(3.4), the random quantities $\{u_n(r,\theta,y)\}$ in (3.3) are expanded by gPC expansion

$$u_n(r,\theta,y(\omega))\approx\sum_{m=1}^{M}\hat{u}_{n,m}(r,\theta)\Phi_m(y(\omega)), \qquad n=0,1,\ldots,\infty. \tag{3.13}$$

By applying the stochastic Galerkin procedure to system (3.4), we obtain, for $n=0,\ldots,n_{\max}$, $m=1,\ldots,M$,

$$D_r^2\hat{u}_{n,m}+\partial_\theta^2\hat{u}_{n,m}+r^2k^2\hat{u}_{n,m}=\hat{F}_{n,m}(r,\theta), \qquad (r,\theta)\in D_{a,b}, \tag{3.14a}$$

$$\hat{u}_{n,m}(a,\theta)=\delta_{n,0}\delta_{m,0}\xi(\theta), \tag{3.14b}$$

$$\partial_r\hat{u}_{n,m}(b,\theta)-T\hat{u}_{n,m}(b,\theta)=\hat{J}_{n,m}(\theta), \tag{3.14c}$$

where

$$\hat{F}_{n,m}=\int_\Gamma F_n(r,\theta,y)\Phi_m(y)\rho(y)dy, \quad \text{and} \quad \hat{J}_{n,m}=\int_\Gamma J_n(\theta,y)\Phi_m(y)\rho(y)dy \tag{3.15}$$

are the gPC coefficients for $\{F_n\}$ and $\{J_n\}$, respectively. Note that $\{\hat{u}_{n,m}\}$ are deterministic quantities and problem (3.14) is a set of deterministic equations.

3.2.2 gPC collocation approach for source terms

The coefficients $\{F_n\}$ and $\{J_n\}$ take rather complicated form, as shown in (3.4d) and (3.4e). Hence, analytical evaluations of their gPC expansion coefficients, $\{\hat{F}_{n,m}\}$ and $\{\hat{J}_{n,m}\}$ in (3.15), are not straightforward, if not impossible. To circumvent this difficulty, we employ the stochastic collocation technique, where the integrals in (3.15) are approximated by the following summation,

$$\hat{F}_{n,j}\approx\sum_{k=1}^{Q_n}F_n(r,\theta,y_k)\Phi_j(y_k)w_k, \tag{3.16}$$

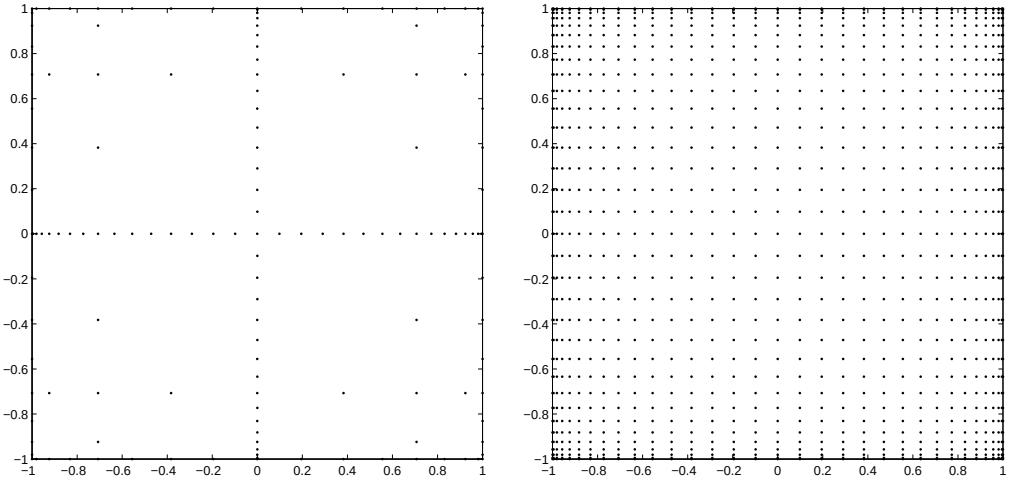

Figure 1: Two-dimensional ($N=2$) nodes based on the extrema of Chebyshev polynomials. Left: Sparse grid from Smolyak algorithm. Total number of points is 145. Right: Tensor product grid constructed from the same one-dimensional nodes. Total number of nodes is 1,089.

and

$$\hat{J}_{n,j} \approx \sum_{k=1}^{Q_n} J_n(\theta, y_k)\Phi_j(y_k)w_k, \tag{3.17}$$

where $\{y_k, w_k\}_{j=1}^{Q_n}$ are a set of nodes and weights in the N-dimensional space Γ.

Although there are plenty of choices for the nodal set in one dimensional random space (N=1), e.g., quadrature rules, it is more difficult to design an efficient nodal set in higher dimensions (N>1). A simple tensor product of one-dimensional quadratures is impractical as the total number of nodes grows too fast for $N \gg 1$. (With tensor product, a one-dimensional nodal set with m nodes will have m^N nodes in N-dimensional space.) It was shown in [27] that the collocation nodes defined by Smolyak sparse grids ([23]) are particularly efficient for stochastic equations — the number of nodes depends weakly on the dimension of the random space, and the integration orders, i.e., polynomial exactness, can be refined to arbitrarily high orders. Hence, we will use the sparse grid to approximate integrals (3.15) via (3.16)–(3.17). For a systematical study of high-order stochastic collocation methods, we refer to [27]. An example of sparse grid and tensor grid in two-dimensional space is illustrated in Fig. 1.

3.3 Spectral Galerkin approximation in physical space

The equations for the gPC coefficients in (3.14) are a set of *deterministic* Helmholtz equations in an annular domain with the non–standard outer boundary condition (expressed using a Dirichlet–Neumann operator). Since the equation (3.14) has to be solved for multiple $((n_{\max}+1)\times M)$ number of times, it is very important to employ an efficient and accurate algorithm for (3.14). Since the equation (3.14) is set on a fixed annulus, it is

natural to use a spectral method. We now briefly describe the spectral–Galerkin method developed very recently in [14] for the following problem (which is slightly more general than (3.14a)–(3.14c)):

$$D_r^2 U+\partial_\theta^2 U+r^2k^2U=G, \qquad (r,\theta)\in D_{a,b}, \tag{3.18a}$$

$$U(a,\theta)=\zeta(\theta), \tag{3.18b}$$

$$\partial_r U(b,\theta)-TU(b,\theta)=\eta(\theta), \tag{3.18c}$$

where $G(r,\theta)$, $\zeta(\theta)$ and $\eta(\theta)$ are given functions. The key observation is that the DNO T defined in (2.3), while global in physical space, is local in Fourier coefficient space. Hence, substituting $U(r,\theta)$, $G(r,\theta)$, $\zeta(\theta)$ and $\eta(\theta)$ in (3.18) by their Fourier expansion, i.e.,

$$(U(r,\theta),G(r,\theta))=\sum_{p=-\infty}^{\infty}(\hat{u}_p(r),\hat{g}_p(r))e^{ip\theta}, \quad (\zeta(\theta),\eta(\theta))=\sum_{p=-\infty}^{\infty}(\hat{\zeta}_p,\hat{\eta}_p)e^{ip\theta},$$

and using (2.3), we can decompose (3.18) into the following sequence of one–dimensional problems ($p=0,\pm1,\pm2,\ldots$):

$$D_r^2\hat{u}_p+(r^2k^2-p^2)\hat{u}_p=\hat{g}_p, \qquad r\in(a,b), \tag{3.19a}$$

$$\hat{u}_p(a)=\hat{\zeta}_p, \tag{3.19b}$$

$$\partial_r\hat{u}_p(b)-k\frac{d_zH_p^{(1)}(kb)}{H_p^{(1)}(kb)}\hat{u}_p(b)=\hat{\eta}_p, \tag{3.19c}$$

which can then be efficiently solved by using a spectral-Galerkin method. More precisely, assuming N_r and N_θ are the number of points used in the radial and azimuthal directions, then the total number of operations needed for solving the equation (3.18) is a small multiple of $N_r^2N_\theta\log(N_\theta)$. We refer to [14] for a detailed description of this algorithm.

4 Numerical examples

In this section we provide numerical examples to examine the accuracy and efficiency of the present algorithm. Our focus here is two-dimensional scattering over bounded obstacles with rough surfaces.

4.1 Acoustic scattering of rough cylinders

We first consider scattering of a cylinder with uncertain rough surfaces.

4.1.1 A model problem

We first present numerical results of a diagnostic case, whose exact solution is available. We consider a cylinder with uncertain surface height of the form $r_a(\theta,y)=a+g(\theta,y)$ where

$g(\theta,y)=\varepsilon y f(\theta)$, with $y(\omega)\in(-1,1)^N$ a N-variate random vector uniformly distributed in $(-1,1)^N$, and $\varepsilon>0$ a real parameter controlling the level of uncertainty. We construct an exact solution of the form

$$v_p(r,\theta,y)=a_p H_p^{(1)}(kr(y))e^{ip\theta} \tag{4.1}$$

by setting the boundary condition

$$\xi(\theta,y)=v_p(r_a(\theta,y),\theta).$$

Hence, when $(\varepsilon,f(\theta),\xi)$ are provided, the stochastic TFE algorithm can deliver approximations to the field to be compared with the exact field, v_p. To test numerical results, we focus on the surface current at the obstacle, where the effects of geometric perturbations are felt most strongly. The surface current is defined as

$$\nu(\theta,y)=\nabla v|_{r=r_a}\cdot N_g,$$

where $N_g=((a+g),-\partial_\theta g)^T$ is chosen unnormalized to match the definition of the Dirichlet–Neumann operator (DNO) (see [8,12,13]). Subsequently,

$$\nu(\theta,y)=(a+g)\,\partial_r v|_{r=r_a}-\frac{(\partial_\theta g)}{(a+g)}\,\partial_\theta v|_{r=r_a}. \tag{4.2}$$

In the first test, we set $f(\theta)=\cos(\theta)$, $\varepsilon=0.05$, and $N=1$. We employ stochastic collocation with 8^{th}-order accuracy in random space to evaluate the complicated right-hand-side of (3.16) and (3.17) in order to ensure the errors induced by stochastic collocation is subdominant. In physical space, we use grid of $N_r=64$ and $N_\theta=32$, and employ 10^{th}-order TFE expansion. Such resolutions are chosen based on comprehensive numerical tests and yield errors in physical space of order $\mathcal{O}(10^{-10})$.

Fig. 2 shows the mean-square error convergence with increasing orders of gPC expansion. The mean-square errors are defined as

$$\epsilon^2=\mathbb{E}[(\nu-\nu_{exact})^2]=\int_\Gamma(\nu-\nu_{exact})^2\rho(y)dy,$$

and the integral is again evaluated by the collocation procedure as in Section 3.2.2. The error convergence with respect to the order of gPC expansion is shown in Fig. 2, and we observe an exponential convergence as the order of expansion increases. Such fast convergence is common for gPC expansion when the solution is sufficiently smooth in random space.

4.1.2 Rough random surface

To model a more realistic random surface on a circle, we employ a Fourier expansion for a periodic random process $\widetilde{f}(t,\omega)$, i.e.,

$$f(t,\omega)=\sum_{n=-K}^{K}f_n(\omega)e^{-int} \tag{4.3}$$

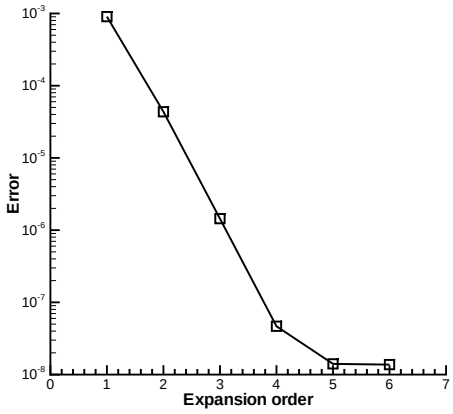

Figure 2: Mean square errors of model case with increasing order of gPC expansions.

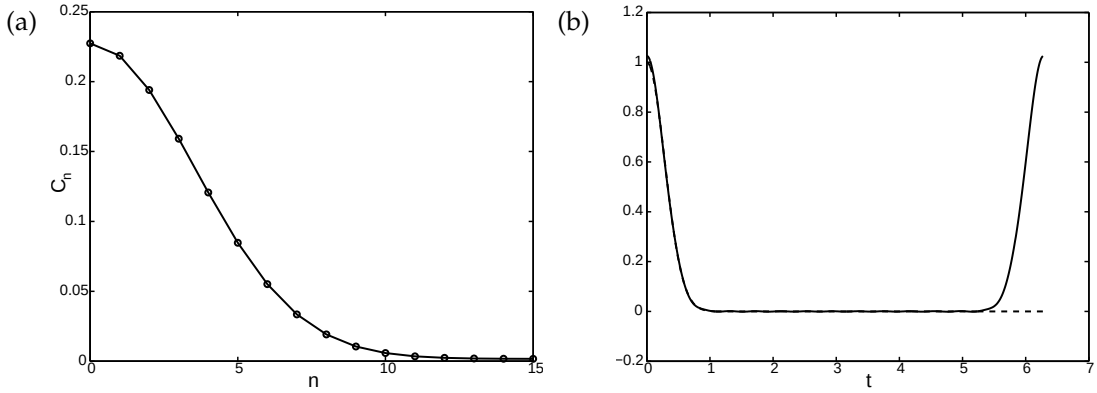

Figure 3: Construction of a 2π-periodic covariance function C_f. (a) Decay of Fourier cosine coefficients $C_n, n=0,1,\cdots$; (b) Reconstructed periodic covariance function (solid line) by extending the regular Gaussian covariance function (dashed line) $C_G(t)=\exp(t^2/b^2)$ with correlation length $b=0.4$.

Here, the coefficients $f_n(\omega)=f_n^r(\omega)+if_n^i(\omega)$ are complex random variables. It is straightforward to show that if f_n^r and f_n^i are statistically independent for all n, and have zero mean and variance of $C_n/4$, where $C_n=\frac{1}{\pi}\int_0^{2\pi}C_{\widetilde{f}}(t)\cos(nt)dt$ are the coefficients of the Fourier cosine series of the 2π-periodic covariance function $C_{\widetilde{f}}$, then the random field $f(t,\omega)$ given by (4.3) approximates the prescribed 2π-periodic covariance function $C_f\to C_{\widetilde{f}}$ as $K\to\infty$. Let $y(\omega)=(f_0^r,f_1^r,f_1^i,\cdots,f_K^r,f_K^i)$, then $f(t,\omega)\equiv f(t,y(\omega))$ has $(2K+1)$ random dimensions. (Note that $f_0^i=0$ for f real.) Obviously, $f(t,y(\omega))$ is an approximation of $\widetilde{f}(t,\omega)$, as (4.3) is a finite-term summation. In practice, we choose the number of expansion terms so that the contributions from the truncated terms are sufficiently small.

In this numerical example, we choose a 2π-periodic covariance function C_f by extending the standard Gaussian covariance function $C_G(t)=\exp(-t^2/b^2)$ to the periodic domain $(0,2\pi)$, where b is the correlation length. Hereafter we choose a moderately

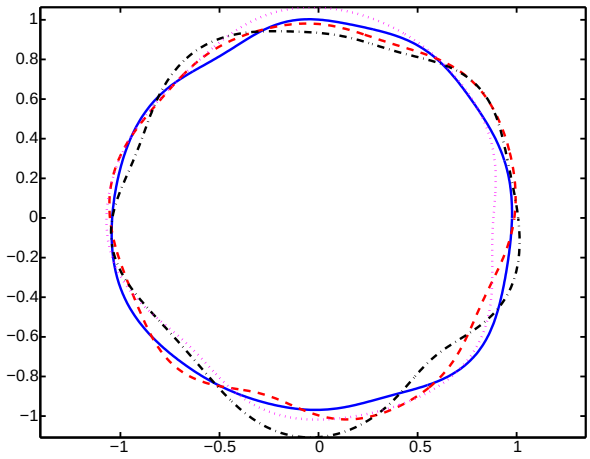

Figure 4: Realizations of rough circular surface generated with the 17-term ($N=17$) Fourier expansion (4.3).

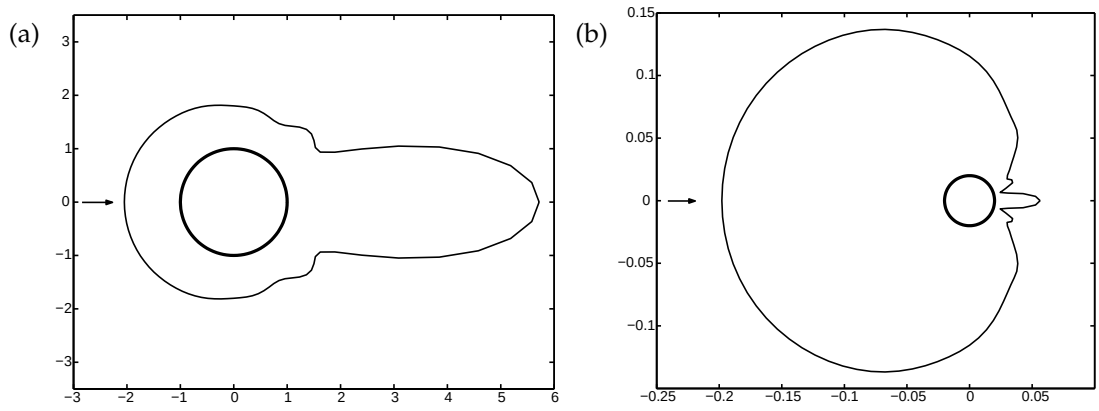

Figure 5: Acoustic scattering over cylinder with rough surface. The arrow indicates the direction of the incident plane wave. (a) The mean solution of RCS. The thick circle is the mean boundary of the scatterer; (b) Standard deviation of the RCS profile. Here the thick circle is only a reference of the location of the cylinder because of the scale difference.

short correlation length $b=0.4$. In Fig. 3(a), the decay of the Fourier cosine coefficient of $C_{\tilde{f}}$ is shown. Due to the relatively fast decay of these coefficients, we choose to use $K=8$ in the truncated series (4.3). Thus, $f(t,y)$ has $N=2K+1=17$ random dimensions. The constructed covariance function $C_f(t)$ is shown in Fig. 3(b), along with the standard non-periodic Gaussian covariance function C_G.

Fig. 4 shows four (arbitrarily chosen) realizations of $f(t,y)$, constructed by N=17 (K=8) dimensions with correlation length b=0.4 and ε=0.1.

An incident plane wave of the form $v^{inc}=\exp(ikx)$ with $k=5$ is introduced. We examine the bistatic radar cross section (RCS) defined as (in two spatial dimensions)

$$s(\theta,y)=\lim_{r\to\infty}2\pi r\frac{|v|}{|v^{inc}|}.$$

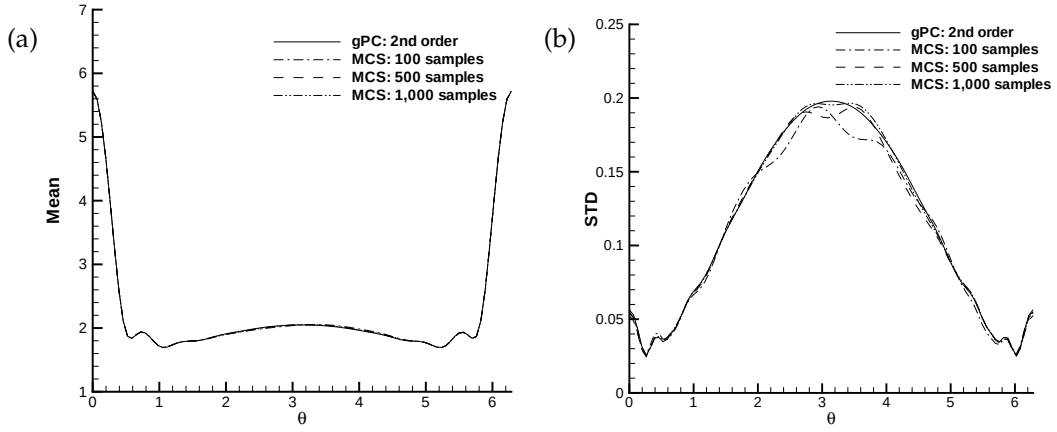

Figure 6: RCS profile of scattering over a rough cylinder. (a) Mean; (b) standard deviation.

In all the following computations, the fixed computational domain is the annulus $D_{a,b}$ with $a=1$ and $b=10$. Extensive resolution independence tests were conducted and the reported results are produced with $N_r=128$, $N_\theta=96$ in physical domain (see Section 3.3), $n_{\max}=10$ for the order of TFE expansion (see (3.3)), and $P=2$ for the order of gPC expansion (see (3.13)). With random dimension of $N=17$, 2nd-order gPC has $M=171$ expansion terms (see (3.8)) for each $\{u_n\}$ in (3.13).

In Fig. 6, the mean profile of RCS is shown, along with its standard deviation (STD) in Cartesian coordinates. For reference purpose, a rescaled circle, representing the mean shape of the obstacle, is drawn to indicate the location of the cylinder. While the mean RCS does not deviate too much from the corresponding deterministic case, we observe a much larger standard deviation in the back-scattering direction — suggesting that the surface uncertainty has more pronounced effects in back-scattering. To validate the results, we also conducted Monte Carlo simulations (MCS) for the same problem. Comparisons of mean and standard deviation of RCS are shown in Fig. 5 in polar coordinates. We observe a good agreement between the two approaches, and the standard deviation using MCS converges to that using gPC as the number of realizations in MCS increased from 100, 500, to 1,000. (We recall that 171 expansion terms is used in gPC.)

4.2 Acoustic scattering of rough oscillatory-shaped objects

We now simulate a plane wave scattering over a gear-shaped obstacle with uncertain surfaces. Here the surface is constructed as $r_a(\theta,y)=1+\varepsilon[\cos(16\theta)+\sigma f(\theta,y)]$, where $f(\theta,y)$ is the same periodic random process generated in (4.3). Fig. 7 shows the mean and STD profile of RCS, with $\varepsilon=0.1$ and $\sigma=0.2$. Again, for reference purpose, a rescaled mean shape of the rough gear is drawn to indicate the location of the obstacle. Again we observe enhanced uncertainty (STD) in RCS in back-scattering. The STD weakens in the direct back-scatter direction around $\theta=\pi$. Comparisons of mean and standard deviation

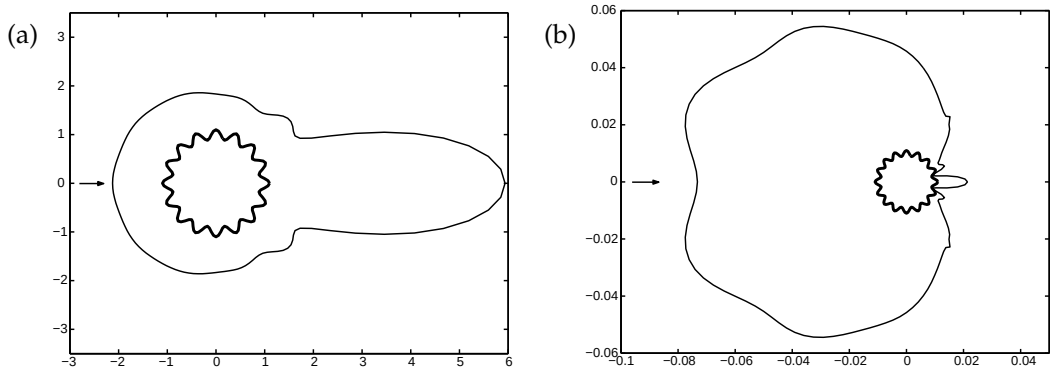

Figure 7: Acoustic scattering over cylinder with rough surface. The arrow indicates the direction of the incident plane wave. (a) The mean solution of RCS. The thick line is the mean boundary of the gear-shaped obstable; (b) Standard deviation of the RCS profile. Here the thick line is only a reference of the location of the obstable because of the scale difference.

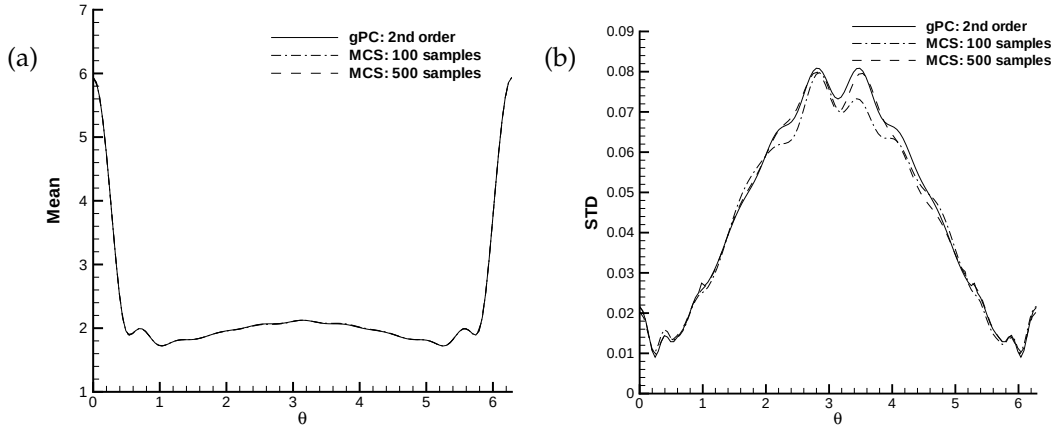

Figure 8: RCS profile of scattering over a rough gear-shaped obstacle. (a) Mean; (b) standard deviation.

of RCS against MCS are shown in Fig. 8 in polar coordinates. We observe good agreements and the convergence of MCS results, as the number of realizations increases, to the converged gPC results.

5 Summary

In this paper we presented an efficient method for scattering problems over bounded rough surfaces. The surface roughness is modeled as random processes, and the governing equation, i.e., Helmholtz equation, is casted in a stochastic framework. The transformed field expansion (TFE) is employed to express the solution as a series expansions of boundary perturbations. The resulting (stochastic) equations are a set of recursive Helmholtz equations for the expansion coefficients. As a result, the original determinis-

tic Helmholtz equation in a random domain is transformed into a set of stochastic equations in a fixed domain. Our numerical discretization is a unified spectral method. The generalized polynomial chaos (gPC) representation in properly defined random space is employed, and a stochastic Galerkin and collocation methods are used to convert the governing stochastic equations into a set of deterministic equations. A highly efficient Fourier-Legendre Galerkin method is then employed to solve the resulting deterministic equations.

We carried out numerical simulations for acoustic wave scattering over a cylindrical and a gear-like shapes with rough surfaces. Exponential error convergence is obtained for a model problem whose exact solution is available. For more realistic rough surface models, we employed Monte Carlo simulations to validate our computational results. Good agreements are obtained at much lower computational cost compared to Monte Carlo sampling.

More in-depth analysis, especially regarding the efficiency of the method with respect to the boundary regularity, and extension to three-dimensional obstacle are under investigation.

Acknowledgments

The work of the second author is supported in part by NSF grants DMS-0243191 and DMS-0311915.

References

[1] I. Babuška, R. Tempone and G. Zouraris, Galerkin finite element approximations of stochastic elliptic differential equations, SIAM J. Numer. Anal., 42 (2004), 800–825.
[2] O. P. Bruno and F. Reitich, Solution of a boundary value problem for the Helmholtz equation via variation of the boundary into the complex domain, Proc. Roy. Soc. Edinburgh Sect. A, 122 (1992), 317–340.
[3] Q.-Y. Chen, D. Gottlieb, and J. Hesthaven, Uncertainty analysis for the steady-state flows in a dual throat nozzle, J. Comput. Phys., 204 (2005), 387–398.
[4] P. Frauenfelder, C. Schwab and R. Todor, Finite elements for elliptic problems with stochastic coefficients, Comput. Meth. Appl. Mech. Eng., 194 (2005), 205–228.
[5] R. Ghanem and P. Spanos, Stochastic Finite Elements: A Spectral Approach, Springer-Verlag, 1991.
[6] O. Le Maitre, O. Knio, H. Najm and R. Ghanem, Uncertainty propagation using Wiener-Haar expansions, J. Comput. Phys., 197 (2004), 28–57.
[7] M. Loève, Probability Theory, 4th ed., Springer-Verlag, 1977.
[8] D. P. Nicholls and N. Nigam, Exact non-reflecting boundary conditions on general domains, J. Comput. Phys., 194 (2004), 278–303.
[9] D. P. Nicholls and F. Reitich, A new approach to analyticity of Dirichlet-Neumann operators, Proc. Roy. Soc. Edinburgh Sect. A, 131 (2001), 1411–1433.
[10] D. P. Nicholls and F. Reitich, Stability of high-order perturbative methods for the computation of Dirichlet-Neumann operators, J. Comput. Phys., 170 (2001), 276–298.

[11] D. P. Nicholls and F. Reitich, Analytic continuation of Dirichlet-Neumann operators, Numer. Math., 94 (2003), 107–146.
[12] D. P. Nicholls and F. Reitich, Shape deformations in rough surface scattering: Cancellations, conditioning, and convergence, J. Opt. Soc. Am. A, 21 (2004), 590–605.
[13] D. P. Nicholls and F. Reitich, Shape deformations in rough surface scattering: Improved algorithms, J. Opt. Soc. Am. A, 21 (2004), 606–621.
[14] D. P. Nicholls and J. Shen, A stable high-order method for two-dimensional bounded-obstacle scattering, SIAM J. Sci. Comput., 28 (2006), 1398–1419.
[15] B. Oksendal, Stochastic Differential Equations. An Introduction with Applications, Springer-Verlag, fifth edition, 1998.
[16] L. Rayleigh, On the dynamical theory of gratings, Proc. Roy. Soc. London, A79 (1907), 399–416.
[17] S. O. Rice, Reflection of electromagnetic waves from slightly rough surfaces, Comm. Pure Appl. Math., 4 (1951), 351–378.
[18] S. Sakamoto and R. Ghanem, Simulation of multi-dimensional non-gaussian non-stationary random fields, Prob. Eng. Mech., 17 (2002), 167–176.
[19] J. Shen, Efficient spectral-Galerkin method. I. Direct solvers of second- and fourth-order equations using Legendre polynomials, SIAM J. Sci. Comput., 15 (1994), 1489–1505.
[20] J. Shen, Efficient spectral-Galerkin method. II. Direct solvers of second- and fourth-order equations using Chebyshev polynomials, SIAM J. Sci. Comput., 16 (1995), 74–87.
[21] J. Shen, Efficient spectral-Galerkin methods. III. Polar and cylindrical geometries, SIAM J. Sci. Comput., 18 (1997), 1583–1604.
[22] M. Shinozuka and G. Deodatis, Simulation of stochastic processes by spectral representation, Appl. Mech. Rev., 44 (1991), 191–203.
[23] S. Smolyak, Quadrature and interpolation formulas for tensor products of certain classes of functions, Soviet Math. Dokl., 4 (1963), 240–243.
[24] D. Tartakovsky and D. Xiu, Stochastic analysis of transport in tubes with rough walls, J. Comput. Phys., in press.
[25] K. F. Warnick and W. C. Chew, Numerical simulation methods for rough surface scattering, Waves Random Media, 11 (2001), R1–R30.
[26] N. Wiener, The homogeneous chaos, Amer. J. Math., 60 (1938), 897–936.
[27] D. Xiu and J. Hesthaven, High-order collocation methods for differential equations with random inputs, SIAM J. Sci. Comput., 27 (2005), 1118–1139.
[28] D. Xiu and G. Karniadakis, Modeling uncertainty in steady state diffusion problems via generalized polynomial chaos, Comput. Methods Appl. Math. Engrg., 191 (2002), 4927–4948.
[29] D. Xiu and G. Karniadakis, The Wiener-Askey polynomial chaos for stochastic differential equations, SIAM J. Sci. Comput., 24 (2002), 619–644.
[30] D. Xiu and G. Karniadakis, Modeling uncertainty in flow simulations via generalized polynomial chaos, J. Comput. Phys., 187 (2003), 137–167.
[31] D. Xiu and D. Tartakovsky, Numerical methods for differential equations in random domain, SIAM J. Sci. Comput., 2006, in press.
[32] F. Yamazaki and M. Shinozuka, Digital generation of non-Gaussian stochastic fields, J. Eng. Mech., 114 (1988), 1183–1197.